JGR Space Physics

RESEARCH ARTICLE
10.1029/2020JA028717

Simultaneous Observation of an Auroral Dawn Storm With the Hubble Space Telescope and Juno

B. G. Swithenbank-Harris[1], J. D. Nichols[1], F. Allegrini[2,3], F. Bagenal[4], B. Bonfond[5], E. J. Bunce[1], G. Clark[6], W. S. Kurth[7], B. H. Mauk[6], and R. J. Wilson[4]

[1]School of Physics and Astronomy, University of Leicester, Leicester, UK, [2]Southwest Research Institute, San Antonio, TX, USA, [3]Physics and Astronomy Department, University of Texas at San Antonio, San Antonio, TX, USA, [4]Laboratory for Atmospheric and Space Physics, University of Colorado Boulder, Boulder, CO, USA, [5]Laboratoire de Physique Atmosphérique et Planétaire, STAR Institute, Université de Liège, Liège, Belgium, [6]Applied Physics Laboratory, The Johns Hopkins University, Laurel, MD, USA, [7]Department of Physics and Astronomy, University of Iowa, Iowa City, IA, USA

Key Points:

- HST images captured a dawn storm while Juno was present in Jupiter's dawn outer magnetosphere
- Juno in situ measurements suggest a region of hot, accelerated plasma in the outer magnetosphere following storm onset
- JEDI particle distributions reveal an extended region of energetic particles near the magnetopause following the storm

Correspondence to:
B. G. Swithenbank-Harris,
bgsh1@le.ac.uk

Citation:
Swithenbank-Harris, B. G., Nichols, J. D., Allegrini, F., Bagenal, F., Bonfond, B., Bunce, E. J., et al. (2021). Simultaneous observation of an auroral dawn storm with the Hubble Space Telescope and Juno. *Journal of Geophysical Research: Space Physics*, *126*, e2020JA028717. https://doi.org/10.1029/2020JA028717

Received 21 SEP 2020
Accepted 9 FEB 2021

Abstract On July 13, 2016, the Hubble Space Telescope observed the onset of a dawn storm in Jupiter's northern ultraviolet aurora, while the NASA Juno spacecraft simultaneously traversed the dawnside outer magnetosphere. This represents the first concurrent auroral and in situ magnetospheric observations of the onset of a dawn storm at Jupiter. Mapping the auroral emission to the magnetosphere reveals the dawn storm corresponds to a source region at ~60 Jupiter radii, and the eastward edge propagates toward local noon at speeds exceeding corotation. Particle observations from Jovian Auroral Distributions Experiment (JADE) and Jupiter Energetic particle Detector Instrument (JEDI) reveal the presence of enhanced hot plasma density in the outer magnetosphere during this interval, and pitch angle distributions measured with JEDI reveal pronounced field-aligned proton and heavy ion motion. Juno magnetometer (MAG) signatures reveal a reversal in the azimuthal magnetic field at the time of storm onset, suggesting acceleration of the hot plasma population above typical sub-corotational speeds. JEDI also detects a region of energetic particles which persists throughout the day following the storm, a feature which is not observed during subsequent perijoves. We interpret this dawn storm as the result of reconnection at earlier local times, possibly associated with a disruption of the azimuthal magnetodisk current.

1. Introduction

Jupiter's ultraviolet auroras are dominated by the main auroral oval, an almost continuous narrow band or series of bands of emission encircling the magnetic poles of the planet (e.g., Clarke et al., 2004; Grodent et al., 2003). This emission maps to the middle magnetosphere, and is generally believed to be driven by the breakdown in corotation of iogenic plasma at radial distances of several tens of planetary radii (Cowley & Bunce, 2001; Hill, 2001; Southwood & Kivelson, 2001). While the overall morphology of the main emission is fixed in System-III longitude and is relatively stable over observation timescales (Clarke et al., 2004), there also exist more dynamic features known to develop over timescales of minutes to tens of minutes. An example of these dynamic phenomena is dawn storms, a brightening of the main emission fixed at dawn. These events produce the most powerful auroral emissions observed at Jupiter and are likely associated with significant reconfigurations of the magnetosphere, but the precise mechanisms of their generation and evolution are currently unknown.

Dawn storms were first observed in Jupiter's northern far ultraviolet (FUV) aurora using the Faint Object Camera (FOC) and Wide Field Planetary Camera 2 (WFPC2) on HST (Ballester et al., 1996; Clarke et al., 1998; Gérard et al., 1994), and were characterized as bright enhancements of the dawnward arc of the main emission. These enhancements expand poleward and eastward longitudinally over several tens of minutes, then appear fixed near dawn for several hours before returning to typical auroral intensities. Auroral intensities often peak at several MR to tens of MR, and additionally high color ratios have previously been measured for dawn storm emissions (Gustin et al., 2006), indicating significant hydrocarbon absorption of the auroral emission. This suggests electrons precipitating in the region penetrate to greater depths in the upper atmosphere, requiring higher electron energies than are typically calculated for the

main auroral emission (~100 keV compared to 460 keV for bright dawn emissions (Cowley & Bunce, 2001; Gustin et al., 2006)). Additionally, the association with local time implies a relationship with the solar wind, but observations performed during the New Horizons flyby in 2007 (Clarke et al., 2009; Nichols et al., 2009) and later with Juno (Bonfond et al., 2021) found no correlation between solar wind conditions and the occurrence of dawn storms.

Although the magnetospheric origins and dynamics governing dawn storms remain an open question, it has been suggested that these events may result from reconnection events in the magnetotail (Cowley et al., 2003; Woch et al., 2002). Specifically, Woch et al. (2002) suggested that Galileo measurements of plasma bursts in the post-midnight and dawn sectors of the magnetotail may result in the disruption of the cross-tail current and thus produce significant auroral emission, while Cowley et al. (2003) described a large-scale steady state reconnection process which might directly drive dawn storm emissions. Some similarities exist in the interpretation of Saturnian auroral storms, which are observed to originate along the dawn flank and expand poleward of the main oval, and are thought to result from large-scale flux closure in the magnetotail (Clarke et al., 2005; Cowley et al., 2005; Nichols et al., 2014). However, these large scale reconnection events in Saturn's magnetotail are generally induced by solar wind compressions of the magnetosphere, whereas Jupiter's dawn storms have been observed to be independent of solar wind conditions (Ballester et al., 1996; Clarke et al., 2009; Nichols et al., 2009) and are thus likely internally driven. We also note that internally-driven magnetotail reconnection, and the inward particle bursts described by Woch et al. (2002), have previously been linked to nightside and dawn auroral spots observed poleward of the main emission (Grodent et al., 2004; Radioti et al., 2008, 2010, 2011), with these phenomena feasibly resulting from smaller scale reconnection events.

Following Juno orbital insertion (JOI) in July 2016, the NASA Juno spacecraft traversed the outer magnetosphere along the dawn meridian. During this outbound flight, HST observed Jupiter's FUV auroras over seven orbits (referred to here as "visits") on days of year (DOY) 193–200 of 2016, as shown in Figure 1 and discussed further below. Over much of the interval, the main emissions were significantly enhanced relative to the several hundred kR typically observed for the main emission. From magnetopause and bow shock crossings identified by Hospodarsky et al. (2017), it is known that Juno encountered the dawn magnetopause and bow shock a number of times during this period, suggesting the magnetosphere underwent significant compression with periods of relaxation. In addition to the enhanced emissions throughout this interval, HST observed two dawn storms during this interval, on DOYs 195 and 200. The storm observed on DOY 200 was then followed by an unusual double arc along the dawn main emission, as shown in panel g of Figure 1. We note that an additional dawn observed prior to JOI on DOY 142 (Kimura et al., 2017; Nichols et al., 2017) occurred following compression of the magnetosphere, and was suggested to be initiated by reconnection in the magnetotail.

In this paper, we focus on the onset of the dawn storm on DOY 195. Previous auroral observations of dawn storms have not been supported by in situ spacecraft observations in the outer magnetosphere. Thus, we present the first concurrent remote sensing and magnetospheric in situ observations of a dawn storm onset. We examine both the auroral and in situ observations in detail, identifying several significant features of each, and infer the dynamics operating in the magnetosphere during this interval. Specifically, we show that the storm coincides with a reversal in the azimuthal magnetic field and a dropout in the radial and overall field magnitudes. Juno's particle instruments also show increases in the high energy particle flux simultaneous to these observations, as well as a long-lived hot plasma feature throughout the day following the storm.

2. Data and Analysis

2.1. HST-STIS Observations

The auroral observations discussed here were obtained using the HST Space Telescope Imaging Spectrograph (STIS) on DOYs 193, 195, 196, 199, and 200 as part of HST program GO-14105 (Nichols et al., 2017), with DOYs 195 and 200 each having two visits. FUV time-tagged data was captured utilizing the Multi-Anode Microchannel Array detector, and raw images with a 30 s integration time were extracted from this time tag data with 10 s increments. Throughout the program, the observations used the F25SRF2 filter to remove UV wavelengths corresponding to H Lyman-α emissions, while admitting H_2 Lyman and Werner band

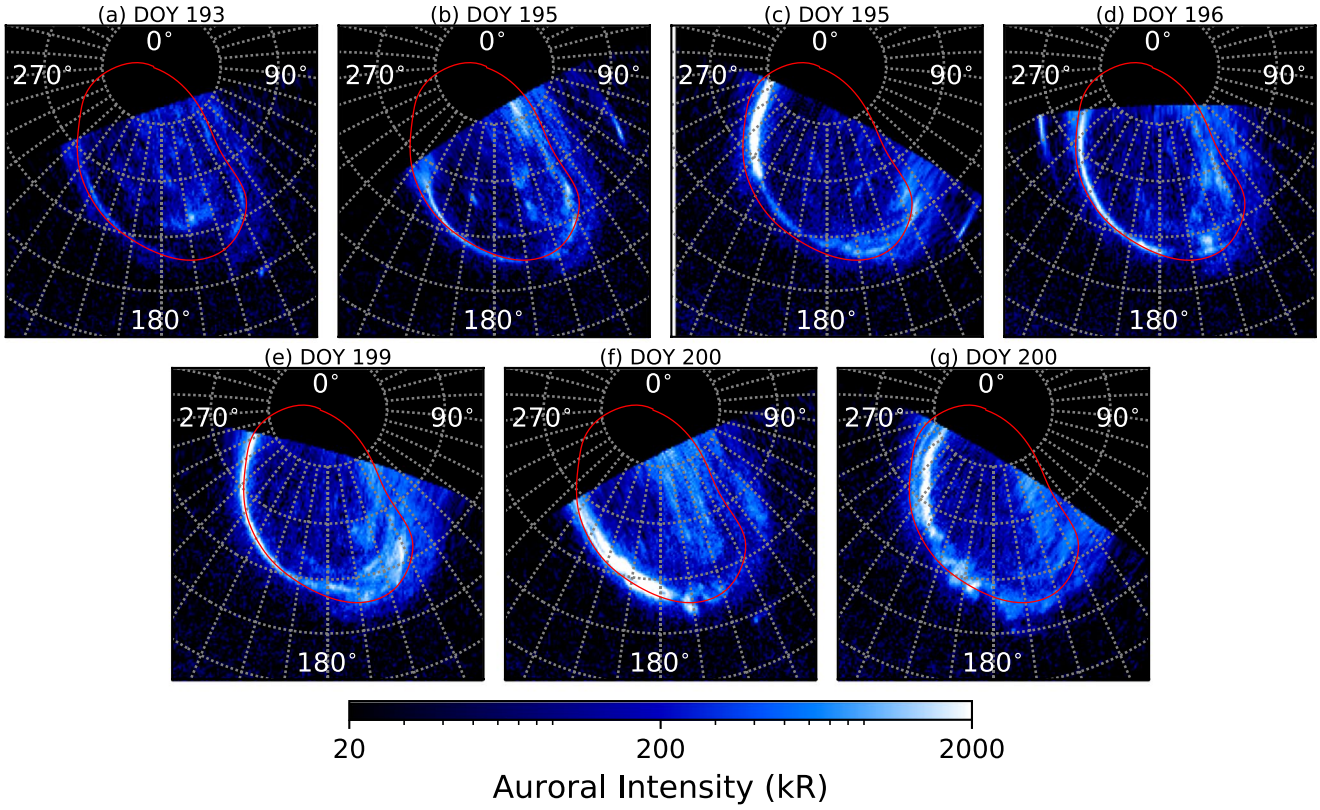

Figure 1. Representative images from the seven HST observation periods during Juno's outbound pass following JOI. All images are of the northern auroral region and have been polar projected using a Lambert azimuthal equal area projection, with 180° System-III longitude fixed at the bottom of each image. A 10° × 10° graticule is overlaid in gray, and the statistical main auroral oval, derived by Nichols et al. (2017), is denoted by the red line. JOI, Juno orbital insertion.

emissions. Raw images were processed with the Boston University pipeline (Clarke et al., 2009; Nichols et al., 2009), and a "standard" color ratio of 2.5 was assumed in converting auroral intensity from counts to kR, using the conversion factors derived by Gustin et al. (2012), though we note that this may underestimate the intensities in the dawn storm region if the color ratio is higher. This choice of color ratio does not affect the morphologies or trends discussed in this paper. All observations are of the northern auroral region, and representative images from each visit are shown in Figure 1.

The evolution of the onset of the DOY 195 dawn storm, highlighted in Figure 1c, is shown in more detail in Figure 2. Observation times are first corrected to account for one-way light travel time between Jupiter and HST to determine the time at which the UV photons were emitted from the ionosphere. Times are then further corrected for the Alfvén travel time from the outer magnetosphere to the ionosphere, estimated by Cowley and Bunce (2003) to be ~18 min at 80 R_J, so the timestamps in Figure 2 represent the time a disturbance propagates in the source region of the magnetosphere. It should be noted that this estimated Alfvén travel time assumes that disturbances apply to the entirety of the current sheet, and thus disturbances propagate from the top of the current sheet to the ionosphere. However, if the propagation time is considered to include traversal of the plasma sheet from its center, the time for Alfvén wave propagation at the radial distances considered here may exceed ~1 h (Bagenal et al., 2017). The 18 min estimate quoted here should thus be thought of as a minimum propagation time between the magnetosphere and ionosphere. This ~40 min uncertainty in Alfvén travel time does not influence any of the conclusions ultimately drawn in this paper since the lifetime of dawn storm auroral events has been previously observed to be several hours (Bonfond et al., 2021; Kimura et al., 2017), i.e. a reasonable fraction of a planetary rotation, and the in situ features discussed here would coincide with the dawn storm in either case.

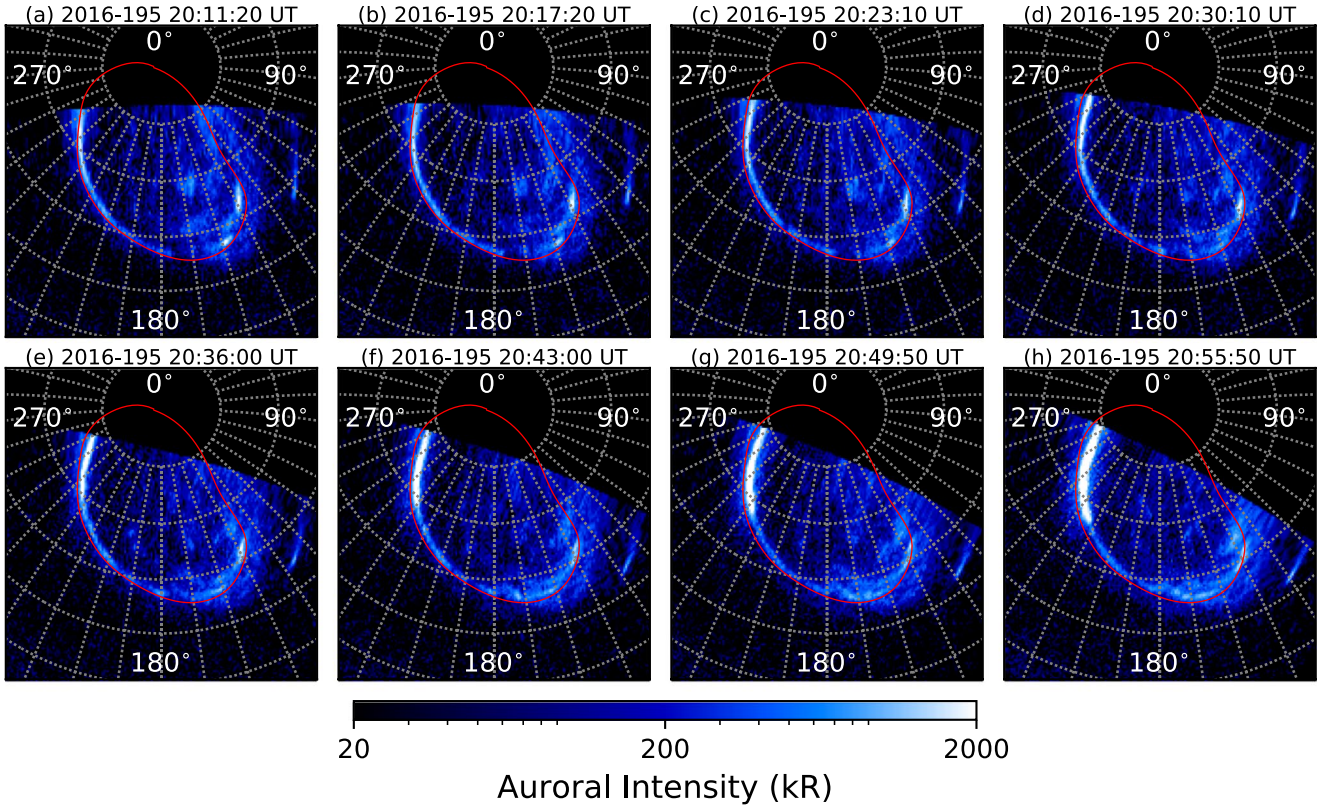

Figure 2. Images from HST Visit 45, showing (a–b) the aurora at the start of the image series, (c–d) early poleward expansion and dawn storm onset, (e–g) noonward expansion and peak intensity, and (h) the end of the image sequence. Images are formatted as in Figure 1, and observation times have been corrected for light travel time and Alfvén propagation to show the expected time a disturbance propagates in the magnetosphere.

At the start of the image sequence shown in Figure 2, the dawn main emission consisted of a narrow, bright arc, which begins to expand poleward and brighten around 20:23 UT (panels c–d of Figure 2). This region of enhanced emission then propagates eastward toward local noon (referred to hereafter as "noonward"), until it dominates the dawn main emission at the end of the visit. The more detailed evolution of this feature will be discussed further below.

2.2. Analysis of Auroral Morphology

A quantitative depiction of the dawn storm, and results from the associated magnetospheric mapping, is displayed in Figure 3. We note that the main emission observed during this visit is shifted slightly poleward of the statistical main oval for this campaign as determined by Nichols et al. (2017). Although not apparent in the peak intensities shown in Figure 3a, the first indication of dawn storm onset occurs at ~20:23 UT with a ~1° expansion of the poleward edge of the main emission and a negligible (0.1°) shift in the equatorward edge of the emission toward the pole, as shown in Figure 3c. The emission peaks at ~8.5 MR about 20 min after the observed storm onset. To compare the local time evolution of the auroral emission with the local time of the associated magnetospheric disturbance calculated below, we utilize the auroral local time (ALT) system defined by Grodent et al. (2004). By then applying an intensity threshold of 1.5 MR to the images to detect the edge of the storm, we observe the noonward expansion occurs more gradually, migrating from 5 to 8 h ALT during the HST observation as shown in panel b. This rate of expansion in local time (approximately 3 h over the ~30 min where the storm is observed) is equivalent to ~250% rigid corotation, or ~1,800 km s^{-1} at 60 R_J, suggesting the magnetospheric source region for the storm is expanding at super-rotational velocities.

We have then mapped the auroral features to the equatorial plane using the flux equivalence method of Vogt et al. (2011) and field line tracing, as shown in Figure 3d. The mapping of the noonward and poleward

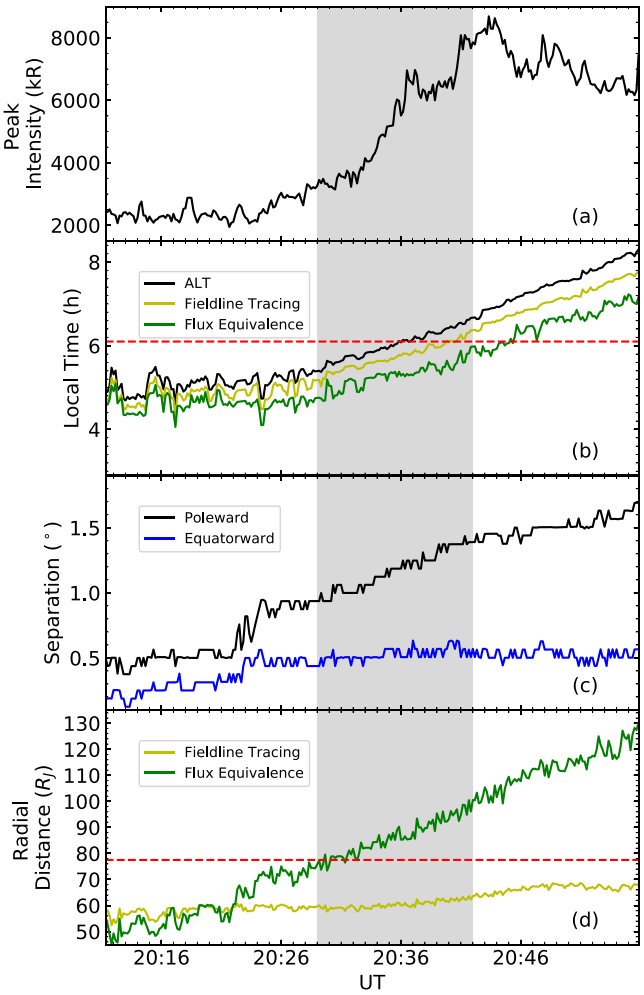

Figure 3. (a) Auroral peak intensity of the dawn main emission, (b) local time of the noonward edge of the dawn storm, (c) mean separation of the storm's poleward (black) and equatorward (blue) edges from the statistical main oval, and (d) the calculated radial distance mapping to this poleward boundary, versus time of the HST observations on DOY 195, corrected for light and Alfvén travel times. The magnetosphere-ionosphere mapping uses the JRM09 internal field and CAN current sheet models (Connerney et al., 1981, 2018), and the green and yellow lines in panels b and d show the results of the Vogt et al. (2011) flux equivalence model and field line tracing respectively. Values of ALT are calculated using the method derived by Grodent et al. (2004). The red dotted lines indicate Juno's position in local time (panel b) and radial distance (panel d) at the time of the HST observations, and the gray shaded region indicates the estimated time of encounter by Juno with the dawn storm source region according to the model results. ALT, auroral local time; DOY, days of year.

edges of the dawn storm to the magnetosphere (Figures 3b and 3d) utilize the JRM09 internal field and CAN current sheet models (Connerney et al., 1981, 2018) for both methods. The local time extent of the dawn storm calculated from both methods agrees closely with the ALT (to within ~30 min) measured from the auroral images. Over the 30 min for which we observe the evolution of the storm, the poleward edge of the storm expands from ~58 R_J to 68 R_J for the field line tracing, and from ~50 R_J to 130 R_J for the flux equivalence method. The significant disparity between the radial distances returned by the two models primarily results from a greater uncertainty in mapping with the field line tracing method beyond ~30 R_J, as discussed by Vogt et al. (2011); Vogt et al. (2015). We note that the ~130 R_J radial distance returned by the flux equivalence method would indicate a majority of the closed magnetosphere in this sector is affected by the dawn storm event. We further note that at the time of the dawn storm, the Juno spacecraft was located near the dawn meridian (6 h LT) at a radial distance of ~77 R_J.

According to the model results, Juno should encounter the magnetospheric source region of the dawn storm between ~ 20:29 and 20:42 UT, thus we may reasonably expect to observe in situ features near this time interval. However, mapping between the magnetosphere and ionosphere beyond 30 R_J is subject to significant uncertainty due to the stretching of the field lines at increasing radial distances. During this interval, the mapping uncertainty is also greater due to the reconfiguration of magnetic field lines occurring as part of the dawn storm, with a 1° shift in the ionosphere corresponding to a shift of a few R_J in the middle magnetosphere with the field line tracing model, or ~20–30 R_J with the flux equivalence model. This result is therefore intended to give a general approximation of the magnetospheric source region of the dawn storm for comparison with the position of the Juno spacecraft.

2.3. Juno In Situ Observations

Turning now to the Juno in situ data, magnetic field and particle observations were obtained using the magnetometer (MAG; Connerney et al., 2017), the Jovian Auroral Distributions Experiment (JADE; McComas et al., 2017), the Jupiter Energetic particle Detector Instrument (JEDI; Mauk et al., 2017), and the plasma waves investigation (Waves, Kurth et al., 2017). The MAG instrument consists of two tri-axial fluxgate magnetometers, fixed on a 4 m long magnetometer boom attached to the end of one of Juno's three solar panel arrays (Connerney et al., 2017). Here we utilize 1 s resolution MAG data in a magnetocentric cylindrical coordinate system. JADE consists of three identical JADE-E sensors measuring electron distributions from ~0.1–100 keV, and one JADE-I sensor measuring ions from ~5 eV to ~50 keV (McComas et al., 2017). The JADE data during the dawn storm interval were obtained in low-rate science (LRS) mode, providing 1 min resolution over most of the period of interest. The JADE-E and JADE-I data utilize the latest in-flight calibrations described by Allegrini et al. (2020) and Kim et al. (2020) respectively, and were used to compute 1D electron and 3D proton, including temperature, density, and velocities. These moments were then resampled at 10 min resolution, and values with an error greater than 200% were excluded.

JEDI is capable of measuring the energy and angular distributions of electrons from ~25 keV to 1.2 MeV, and the energy, angular and compositional distributions of ions from ~10 keV to >1.5 MeV for protons and ~145 keV to >10 MeV for oxygen and sulfur ions (Mauk et al., 2017). Pitch angle distributions are derived

by combining the JEDI particle data with the MAG vector measurements of the local magnetic field. The compositional distributions are only resolved in the JEDI-90 and JEDI-270 sensors since they operate in a time-of-flight by energy (TOFxE) mode which is able to deduce the ion's velocity from the start and stop timing pulses produced as the ion passes through a set of foils. All sensors (JEDI-90, JEDI-180 and JEDI-270) are capable of measuring electrons and total ions via solid-state detectors. Electron SSDs have ∼2 μm of aluminum flashing to shield < 250 keV protons, whereas the ion SSD has no flashing (referred to as "bare detector" here) and is susceptible to both electrons and ions, which we refer to as "total particles" in this paper. Additionally, JEDI-90 and JEDI-270, are mounted on the spacecraft deck with their FOVs along the spin plane to maximize coverage of the field-aligned particles. The JEDI-180 sensor is mounted perpendicular to the spin plan and can provide nearly complete sky coverage over one spacecraft spin (or every 30 s). Waves comprises a single axis electric dipole antenna with its effective axis perpendicular to the spacecraft spin axis and a single axis search coil magnetometer mounted parallel to the spin axis, and is capable of measuring and distinguishing between wave magnetic fields from 50 Hz to 20 kHz and wave electric fields from 50 Hz to 41 MHz (Kurth et al., 2017). From Waves, we primarily focus on the decametric (∼10–40 MHz) and hectometric (∼200 kHz to a few MHz) emission frequencies, and also utilize electron densities derived from the low-frequency cutoff of continuum radiation by the method described by Barnhart et al. (2009).

Figures 4 and 5 display the Juno MAG, JADE, JEDI, and Waves data for DOYs 195–196, and a close up of the dawn storm interval on DOY 195, respectively, with the magnetic field expressed in a cylindrical polar coordinate system. During this interval, Juno remained near 6 h local time and traveled outward from 73.5 to 82 R_J, and the distance from Juno to the center of the current sheet was calculated using the model derived by Khurana (1992),

$$Z_{cs} = \rho \tan(\theta)\left[\frac{x_0}{x}\tanh\frac{x}{x_0}\cos(\lambda - \delta)\right], \tag{1}$$

where θ is the dipole tilt angle, x_0 is the current sheet hinge distance, and δ is the longitude toward which the current sheet tilts. The value of δ is given by

$$\delta = \delta_0 - \frac{\Omega_J \rho_0}{v_0}\ln\left(\cosh\left(\frac{\rho}{\rho_0}\right)\right). \tag{2}$$

where δ_0 is the longitude of the prime meridian, ρ_0 is the radial distance at which wave delay becomes significant, and v_0 is the wave velocity. In this study, we use the values of x_0, v_0, and ρ_0 derived by Khurana and Schwarzl (2005), and θ and δ_0 were calculated using the JRM09 internal magnetic field model (Connerney et al., 2018). Focusing on the wider interval shown in Figure 4, for much of this interval Juno detected consistent negative radial and positive azimuthal field components of ∼−6 and 4 nT respectively, with B_z oscillating due to the motion of Juno through the current sheet field structure over a planetary rotation. This configuration is typical of a "lagging" field in the southern hemisphere. We note that significant departures from this description are present throughout DOY 196 which will be discussed later.

JADE electron and proton temperatures, shown in panel f of Figures 4 and 5, typically vary with a 10-h periodicity over the two days, reaching minimum temperatures of ∼0.3–0.6 keV and 0.5–1.3 keV respectively below the current sheet, and maximum temperatures of ∼2–3 keV and 5–8 keV during current sheet encounters. This periodicity is also suggested in the particle densities derived from both JADE and Waves data (Figures 4g and 5g), with proton and electron densities of 1–2 × 10^{-3} particles/cm^{-3} increasing to 0.9–1 × 10^{-2} particles/cm^{-3} near the current sheet. Electrons and protons of temperatures greater than 50 keV also exhibit this periodicity, with JEDI revealing particle fluxes increasing by factors of ∼2–5 during current sheet approaches. For much of this interval, the counting statistics for heavy ions detected by JADE remain low and return moments with significant error, so these moments are not presented here. We also note that the very low counts observed for energies below ∼1 keV in Figure 4e are the result of a temporary change in JADE's time resolution from 1 min to 10 min around the time of the dawn storm, and should not be considered significant. Finally, three HST visits occurred during this interval: two on DOY 195, the second of which included the dawn storm onset, and one on DOY 196.

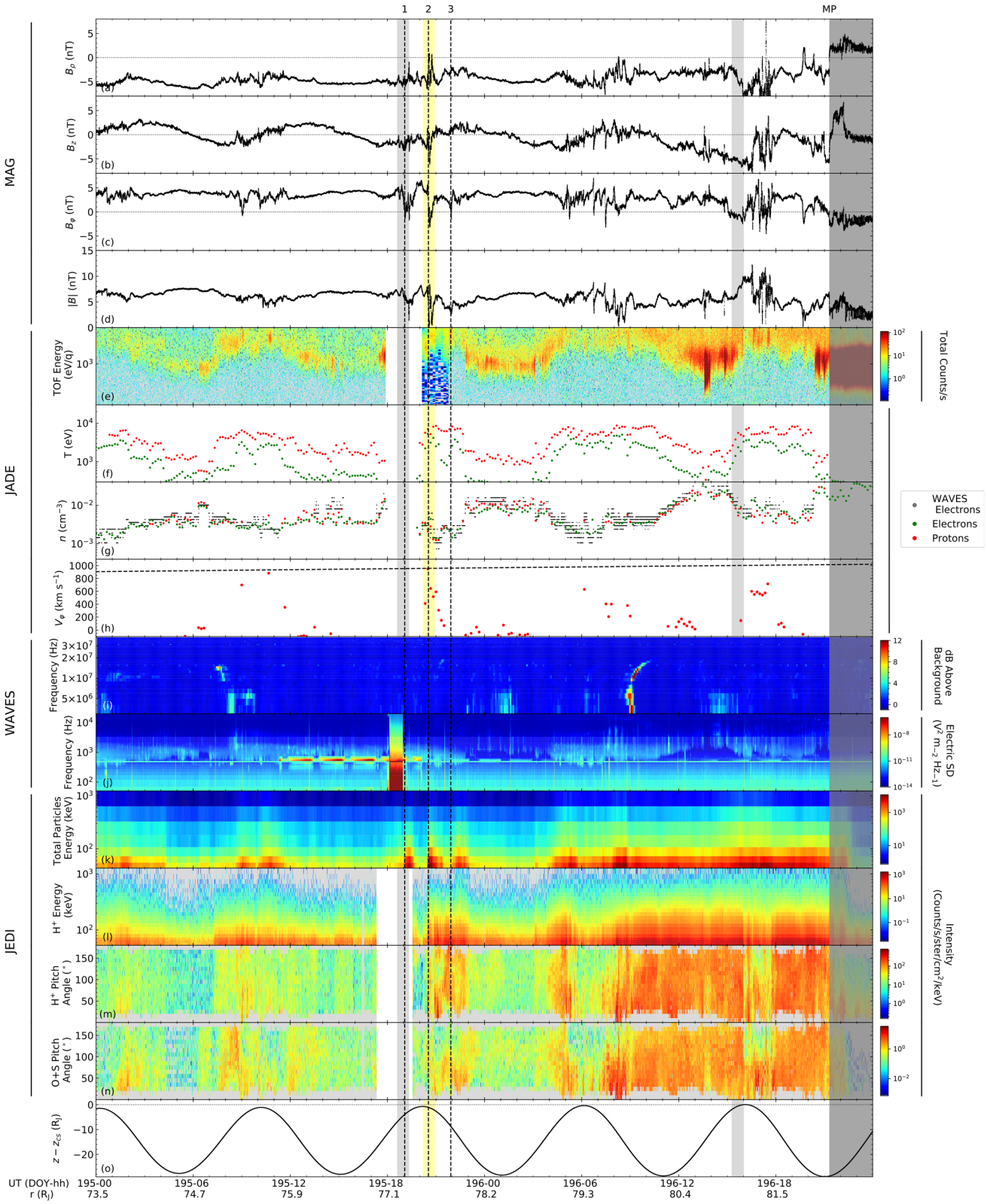
1
2
3
MP
MAG
JADE
WAVES
JEDI
B_ρ (nT)
B_z (nT)
B_φ (nT)
|B| (nT)
TOF Energy (eV/q)
T (eV)
n (cm^{-3})
V_φ (km s^{-1})
Frequency (Hz)
Frequency (Hz)
Total Particles Energy (keV)
H$^+$ Energy (keV)
H$^+$ Pitch Angle (°)
O+S Pitch Angle (°)
$z - z_{cs}$ (R_J)
(a)
(b)
(c)
(d)
(e)
(f)
(g)
(h)
(i)
(j)
(k)
(l)
(m)
(n)
(o)
Total Counts/s
WAVES Electrons
Electrons
Protons
dB Above Background
Electric SD (V^2 m^{-2} Hz^{-1})
Intensity (Counts/s/ster/cm^2/keV)
UT (DOY-hh)
r (R_J)
195-00
73.5
195-06
74.7
195-12
75.9
195-18
77.1
196-00
78.2
196-06
79.3
196-12
80.4
196-18
81.5

On DOY 195, MAG and JEDI exhibit several reversals in the azimuthal magnetic field (dotted lines 1–3 in Figure 4), concurrent with enhancements in the high energy plasma population between 19:00-23:00 UT. Here we focus on the second of these events due to its coincidence with the HST observation of the dawn storm, highlighted by the yellow bar in Figures 4 and 5. Furthermore, JADE and two of the three JEDI detectors were switched off during the first event, while Waves experienced interference from spacecraft gyros between 18:00 and 19:00 UT due to a spacecraft maneuver. Additionally, despite significant FUV emission during this period, Waves detects negligible emission in the decametric and hectometric wavebands, suggesting the spacecraft was out of the beam of auroral radio emission throughout the interval.

Turning then to Figure 5, which focuses on the interval of interest on DOY 195, the magnetometer trace reveals a dropout in the radial and azimuthal magnetic field components from a background magnitude of ∼4–6 nT to ∼ 1 nT, as well as the overall magnetic field strength, starting at ∼20:30 UT. The azimuthal field then reverses for several minutes, peaking at ∼-3 nT, before a more gradual recovery, while the radial field briefly returns to values of 3–6 nT before decreasing again and then gradually recovering to magnitudes of ∼5 nT over 15 min. The radial field strength later decreases again to ∼3 nT approaching another reversal in the azimuthal field. Although Juno is near its closest approach to the current sheet at this time, this configuration of the magnetic field is not typical of a current sheet encounter, as there is no accompanying reversal in the radial field when the azimuthal field reverses in sense. This signature is also distinct from other near-current sheet features such as magnetic nulls (Haynes et al., 1994; Kivelson & Southwood, 2005; Leamon et al., 1995; Southwood et al., 1993), in which the magnetic field strength also decreases to well below the ambient field magnitude, but there is no reversal in the azimuthal field. This reversal of B_φ indicates a transient interval of "leading" field, implying acceleration of plasma above expected subcorotational speeds in this region of the magnetosphere. Furthermore, the sudden decrease in magnetic field strength is consistent with the diamagnetic effect associated with an increase in plasma pressure.

With this in mind, we now turn to the plasma measurements shown in Figures 5k–5n, in which the JEDI bare detector and proton channels exhibit an order of magnitude enhancement in the 50–200 keV energy bands simultaneous with the magnetic signatures described above. As shown in Figures 5e–5g, JADE also detects an increase in proton and electron temperatures to ∼10 and 3 keV respectively at this time, but we note that the densities and temperatures calculated at storm onset are similar to those observed during other current sheet approaches. Additionally, the azimuthal proton velocities, while not exceeding corotational speeds (indicated by the dashed line in Figure 5h), do suggest an acceleration to at least near-corotational velocities at the time of storm onset. We also note that JEDI pitch angle distributions in Figure 5k–5n reveal field-aligned (i.e., southward) motion of protons and heavy ions at storm onset, with an additional significant field-aligned signature appearing at ∼20:50 UT and persisting for tens of minutes. Overall the enhanced proton and ion populations persist until ∼23:00 UT before dropping by a factor of ∼5–10 to near previous fluxes. We note that the JEDI bare detector resolves three distinct enhancements in Figure 4k which coincide with reversals of the azimuthal field, whereas JADE and the other JEDI detectors are unable to clearly resolve these features. Considering the bare detector's sensitivity to both ions and electrons, this indicates an increase in the high energy electron population, although the lack of resolution between electron and ion populations during this interval makes the magnitude of this enhancement unknown.

Another prominent feature in Figure 4 is the extended region of hot (>50 keV) plasma present throughout DOY 196. JADE particle temperatures and JEDI energy and pitch angle distributions are initially enhanced at ∼04:00 UT, and the JEDI distributions in particular remain enhanced until Juno crosses the magnetopause at 21:18 UT, after which the high energy particle fluxes rapidly decrease by 1–2 orders of magnitude.

Figure 4. Juno in situ measurements from DOY 195–196, showing (a–c) the radial, north-south, and azimuthal components of the magnetic field in cylindrical coordinates, in nT, (d) magnetic field strength in nT, (e) JADE ion time-of-flight spectra, (f) electron and proton temperatures, (g) number densities (cm^{-3}), including the Waves electron number densities, and (h) proton azimuthal velocities, with the corotational velocity at increasing radial distances denoted by the dashed line, (i) frequency-time spectrogram of Waves electric field from 4 to 30 MHz and (j) continuum radiation in the Waves electric field channel, (k) JEDI energy distribution for the bare A180 detector, (l and m) proton energy and pitch angle distributions, (n) pitch angle distribution for the oxygen and sulfur energy channels, and (o) the calculated distance between Juno and the center of the current sheet utilizing the model of Khurana (1992). The yellow bar indicates the HST interval during which the dawn storm was observed, and other HST observations during this interval are highlighted in light gray. All HST observation times have been corrected to account for light travel and Alfvén propagation times. The dark gray shading on DOY 196 indicates a magnetopause crossing identified by Hospodarsky et al. (2017). DOY, days of year; JADE, Jovian Auroral Distributions Experiment; JEDI, Jupiter Energetic particle Detector Instrument.

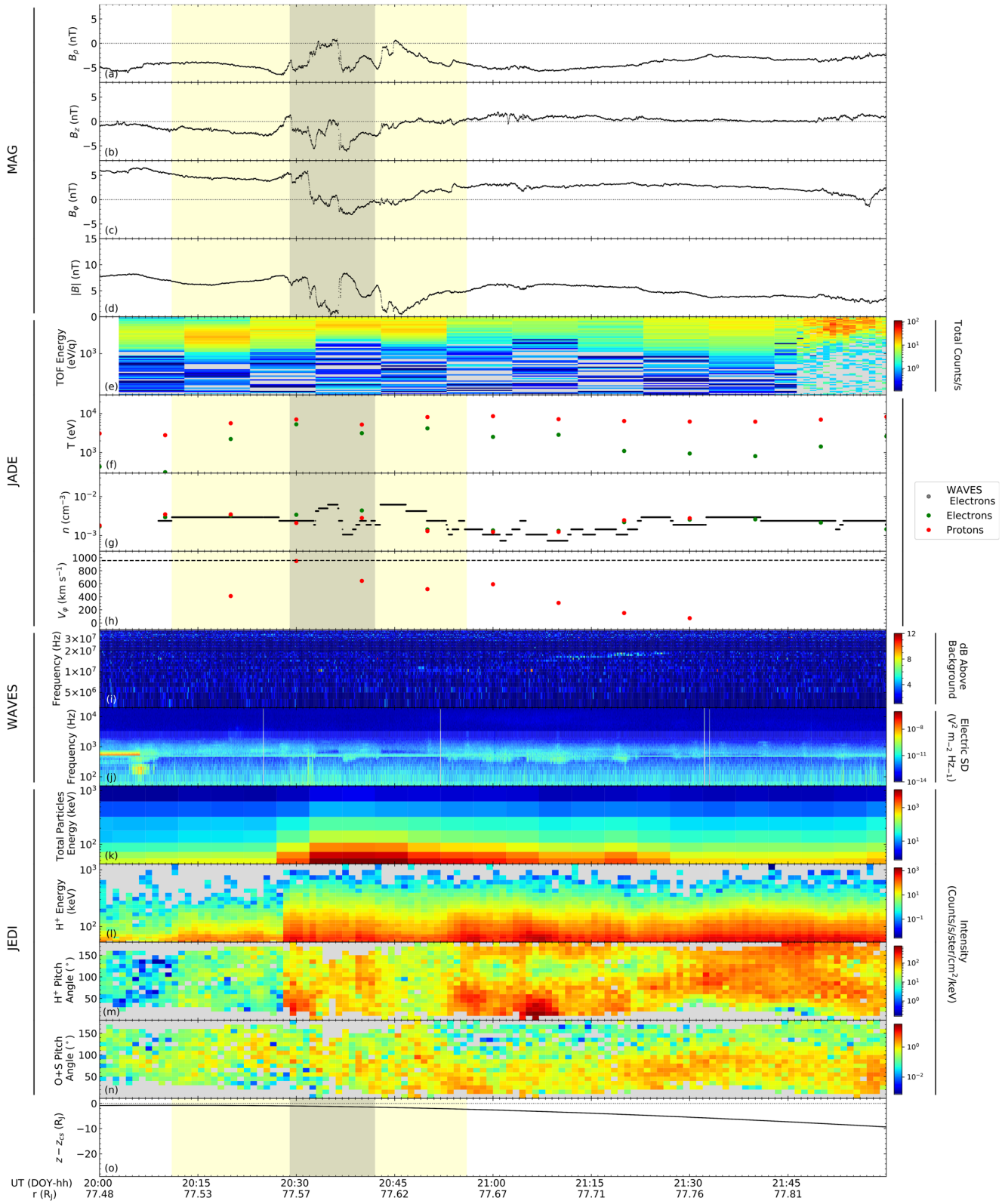

Figure 5. As in Figure 4, but for 20:00–22:00 UT on DOY 195. The gray shaded region indicates the estimated time of encounter by Juno, as shown in Figure 3. As in Figure 4, the yellow shaded region shows the HST observation period during which the dawn storm onset was observed, although the dawn storm is expected to persist for several hours beyond this observation period (Bonfond et al., 2021; Kimura et al., 2017). DOY, days of year.

The minimum lifetime of this hot plasma feature is therefore ~17 h, although the exact lifetime of this region of hot plasma may be significantly greater. Prior to the magnetopause crossing on DOY 196, there is no indication in JADE or JEDI data of the hot plasma beginning to dissipate, and the feature is not observed again when Juno re-enters the magnetosphere at 7:16 on DOY 197 (Hospodarsky et al., 2017), suggesting the true lifetime of this feature is between ~17 and 27 h. MAG signatures also demonstrate significant disturbances in the magnetic field throughout this interval, consistent with a region of hot plasma. We note that these persistent hot plasma populations are primarily present at higher southern magnetic latitudes, extending to ~30 R_J below the current sheet. Reductions of the high energy populations during this interval only occur during current sheet encounters. During these current sheet approaches, the intensity flux drops by roughly an order of magnitude in the 50–200 keV energy range, and proton and ion pitch angle distributions simultaneously become increasingly field-aligned, suggesting the particle motions are primarily southward. Additionally, the auroral emissions observed with HST during this day (Figure 1d), while enhanced compared to typical intensities, show attributes consistent with other HST orbits in this sequence with no clear remnant of the dawn storm remaining in the images.

3. Discussion

Considering now the mechanisms driving the above observations, we first note that the brief reversals of the azimuthal magnetic field, coupled with the JADE azimuthal proton velocities, reveal an acceleration of the thermal plasma toward corotation, significantly faster than the approximately half rigid corotation expected at these radial distances (Kane et al., 1995). Such bursts of fast flow of magnetospheric plasma may result from reconnection at earlier local times accelerating plasma flows along the dawn flank. This region of ongoing reconnection then expands at the local Alfvén speed along the dawn flank, potentially forming the noonward expansion of the auroral emissions at significantly superrotational velocities. The rate of expansion estimated from auroral observations (~1,800 km s−1 at 60 R_J) is comparable with the Alfvén speeds of 1,000–3,000 km s−1 calculated by Bagenal et al. (2017) for a few R_J from the center of the current sheet, where much of the hot plasma is detected by Juno. We note that while the initial reductions in the radial magnetic field may result from proximity to the center of the current sheet, the later gradual decrease corresponds to decreased stretching of the magnetic field lines, indicative of a reconfiguration of the magnetosphere. From arguments made for the terrestrial system, this may be indicative of a disruption of the magnetodisk azimuthal current (Birn & Hesse, 1996; Lui, 1996), although at Earth whether this current disruption precedes reconnection remains unclear (Angelopoulos et al., 2008; Lui, 2009).

The interval on DOY 196 has previously been analyzed by Gershman et al. (2017), who discussed an extended magnetopause boundary layer present in JADE energy and pitch angle spectra and Waves low frequency continuum data which are roughly coincident with the high energy population present in the JEDI distributions discussed above. Gershman et al. (2017) associated this extended boundary region with the mixing of magnetosphere and magnetosheath material. While some of the proton and electron populations observed here could result from a mixing of these regions, the dense oxygen and sulfur populations near the magnetopause boundary will be entirely magnetospheric in origin, as Mauk et al. (2019) revealed that heavier ions such as oxygen and sulfur cannot be easily transported across the magnetopause owing to their increased gyroradii. Furthermore, we do not observe a similarly long-lived hot plasma region near magnetopause crossings or at similar radial distances during other perijoves, such as the interval from PJ1 shown in Figure 6, during which Juno crossed the magnetopause at a similar radial distance and local time to the DOY 196 crossing. We therefore suggest that this enhancement of the high energy plasma population is associated with a reconfiguration of the magnetosphere occurring as part of this dawn storm.

Regarding the ~17 h lifetime of the hot plasma region observed on DOY 196, this timescale is consistent with the lifetime of equatorward emission features resulting from plasma injections into the inner magnetosphere (Badman et al., 2016; Gray et al., 2016). Most notably, Gray et al. (2016) observed a polar spot, possibly driven by magnetotail reconnection, propagate equatorward and merge with the main emission. Equatorward emissions associated with hot plasma injections were observed simultaneously and were still detectable 18 h later, and it was suggested that these injection signatures could be the result of reconnection-driven planetward flows of hot plasma. In the case of the dawn storm, brightening originates along the main emission and propagates poleward, indicating either a radially outward-moving source, or

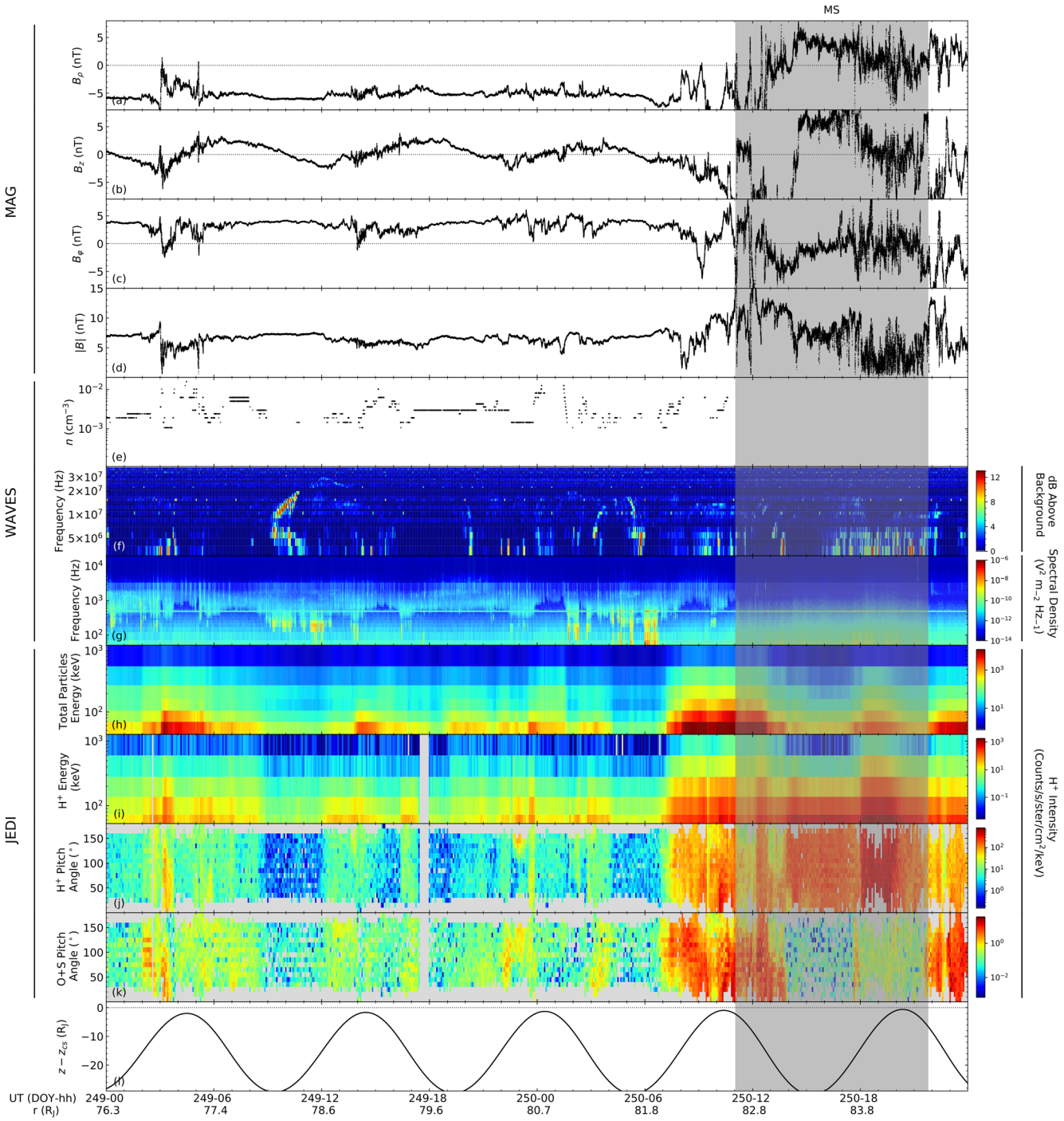

Figure 6. Similar to Figure 4, but for DOY 249–250 of 2016. No JADE data is available from this interval, so only Waves provides an indication of low energy particle density during this interval. The gray shaded region indicates the interval where Juno was located in the magnetosheath as determined by Hospodarsky et al. (2017). DOY, days of year; JADE, Jovian Auroral Distributions Experiment.

reconnection of subsequent flux tubes with increasing vertical distance from the neutral sheet, analogous with the expansion phase of Earth's substorms.

Another parallel between this dawn storm and reconnection-driven polar spots is their superrotational motion in the ionosphere (~250% compared to 270% calculated by Gray et al. (2016)). Additionally, the rapid noonward propagation of the auroral emission is also analogous to the observed propagation of Saturnian

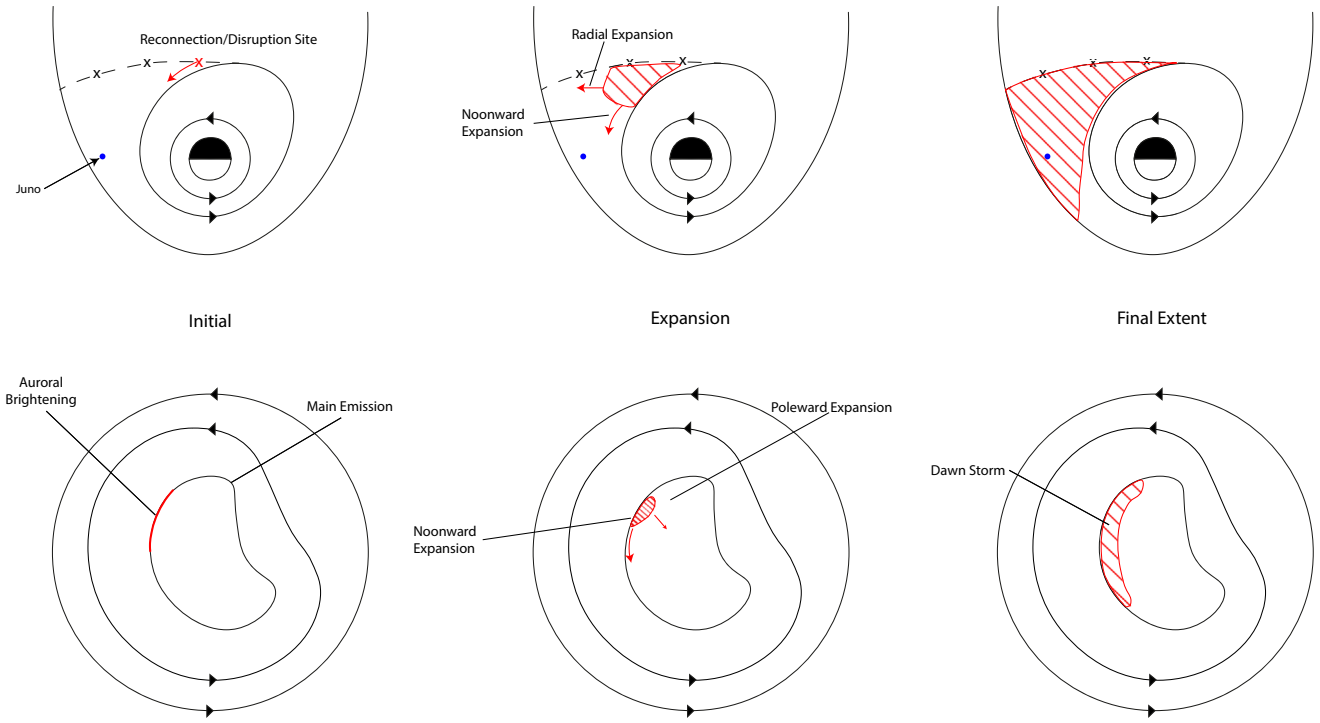

Figure 7. Schematic showing the evolution of the reconfiguration front in the magnetosphere (top) and associated auroral emission (bottom). The blue circle denotes Juno's position in the magnetosphere during the dawn storm, and the red markings highlight regions and features in the magnetosphere and ionosphere expected to correspond to the dawn storm.

storms at superrotational velocities (Nichols et al., 2014). However, Saturnian auroral storms are distinct from Jupiter's dawn storms in that Saturn's storms are likely triggered following magnetospheric compression by the solar wind (Clarke et al., 2005; Cowley et al., 2005; Nichols et al., 2014), whereas Jupiter's storms are observed independent of solar wind conditions (Ballester et al., 1996; Clarke et al., 2009; Nichols et al., 2009). While the enhanced auroral emissions and multiple magnetopause and bow shock encounters by Juno are evidence of significant compression of the magnetosphere throughout this HST campaign, the nature of the solar wind at the time of the dawn storm is not known precisely. Given that the timescale required for the magnetosphere to be compressed is estimated to be on the order of a few hours (Cowley & Bunce, 2003), it is equally feasible that the magnetosphere did not undergo compression until nearly a day after the onset of the storm, with Juno not encountering the magnetopause until 21:18 UT on DOY 196 (Hospodarsky et al., 2017). However, we note that the second dawn storm observed during this HST campaign, on DOY 200, occurred when Juno was in the solar wind and the magnetosphere was compressed. This second storm is reminiscent of a possible poleward boundary intensification (PBI) observed at Saturn (Nichols et al., 2014), which in the terrestrial system result from ongoing reconnection in the magnetotail.

Overall, then, we have shown that this dawn storm was associated with significant plasma dynamics and heating in the dawnside middle to outer magnetosphere, likely initiated by reconnection and/or disruption of the azimuthal current. The schematic in Figure 7 shows the expected generation and evolution of the dawn storm, with reconnection at an earlier local time triggering the reconfiguration of field lines as suggested previously (Kimura et al., 2017; Yao et al., 2020). The reconfiguration front rapidly expands radially outward and through local dawn, corresponding to the poleward and noonward expansion of the auroral emission, until most of the dawn outer magnetosphere is reconfigured at the full extent of the dawn storm.

4. Summary

We have presented the first concurrent magnetospheric and auroral observations of the onset of a dawn storm. HST images obtained on July 13, 2016 showed the onset and early progression of the storm, with a 1° poleward expansion of the main emission corresponding to either a ~10 R_J or ~80 R_J outward expansion of the magnetospheric source region depending upon the mapping model used. The latter result would indicate a major reconfiguration of the majority of closed flux in the dawn magnetosphere. Expansion of the noonward edge of the storm from ~5 to ~8 h LT indicates expansion of the reconnection front at speeds ~250% of rigid corotation, or ~1,800 km s^{-1} at 60 R_J.

Concurrent Juno in situ observations reveal a reversal in the azimuthal magnetic field and dropouts in the radial and overall field magnitudes, as well as dense high energy plasma populations at around the time of storm onset and instances of field-aligned motion of protons and heavy ions during this interval. Throughout the day following the storm, the JEDI instrument also detects a persistent region of hot plasma up to the magnetopause, a feature not detected during later perijoves. The increased particle flux detected during this interval is primarily present at higher latitudes, with decreases in the high energy plasma population being observed during the closest approaches to the current sheet. We therefore associate this dawn storm with the acceleration and heating of magnetospheric plasma following reconnection at earlier local times, possibly associated with a disruption of the magnetodisk current, with the long-lived high energy particle populations being a consequence of the reconfiguration of the magnetosphere following this event.

Data Availability Statement

HST data are available from the MAST Archive (doi: 10.17909/t9-1271-7f52), and Juno data are available from the Planetary Data Server (PDS) at https://pds-ppi.igpp.ucla.edu/. JADE data are from the JNO-J/SW-JAD-3-CALIBRATED-V1.0 data set, version 03 and 02 files for electrons and ions, respectively, and are available from the NASA PDS Archive. MAG data are available from the JNO-J-3-FGM-CAL-V1.0 data set, version 01 files in the PC subdirectory, on the NASA PDS Archive (doi: https://doi.org/10.17189/1519711). JEDI data are from the JNO-J-JED-3-CDR-V1.0 data set, version 04 files, on the NASA PDS Archive. Waves data are from the JNO-E/J/SS-WAV-3-CDR-SRVFULL-V1.0 data set, version 02 files, on the NASA PDS Archive (doi: https://doi.org/10.17189/1520499).

Acknowledgments
This work is based on observations made with the NASA/ESA Hubble Space Telescope (program GO 14105), obtained at STScI, which is operated by AURA, Inc. for NASA. B.G. Swithenbank-Harris was supported by an STFC Studentship. J.D. Nichols and E.J. Bunce were supported by STFC Consolidated Grant ST/N000749/1, and E.J. Bunce was also supported by a Royal Society Wolfson Research Merit Award. The work at the Southwest Research Institute was funded by the NASA New Frontiers Program for Juno. B. Bonfond is a Research Associate of the Fonds de la Recherche Scientifique - FNRS. The authors wish to thank Marissa Vogt for providing the magnetosphere-ionosphere mapping procedure used in this study.

References

Allegrini, F., Mauk, B., Clark, G., Gladstone, G. R., Hue, V., Kurth, W., (2020). Energy flux and characteristic energy of electrons over Jupiter's main auroral emission. *Journal of Geophysical Research: Space Physics*, *125*(4), e2019JA027693. https://doi.org/10.1029/2019JA027693

Angelopoulos, V., McFadden, J. P., Larson, D., Carlson, C. W., Mende, S. B., & Frey, H. (2008). Tail reconnection triggering substorm onset. *Science*, *321*(5891), 931–935.

Badman, S. V., Bonfond, B., Fujimoto, M., Gray, R., Kasaba, Y., Kasahara, S., et al. (2016). Weakening of Jupiter's main auroral emission during January 2014. *Geophysical Research Letters*, *43*(3), 988–997.

Bagenal, F., Adriani, A., Allegrini, F., Bolton, S., Bonfond, B., Bunce, E., et al. (2017). Magnetospheric science objectives of the Juno mission. *Space Science Reviews*, *213*(1–4), 219–287.

Ballester, G. E., Clarke, J. T., Trauger, J. T., Harris, W. M., Stapelfeldt, K. R., Crisp, D., et al. (1996). Time-resolved observations of Jupiter's far-ultraviolet aurora. *Science*, *274*(5286), 409–413.

Barnhart, B., Kurth, W., Groene, J., Faden, J., Santolik, O., & Gurnett, D. (2009). Electron densities in Jupiter's outer magnetosphere determined from Voyager 1 and 2 plasma wave spectra. *Journal of Geophysical Research*, *114*(A5). https://doi.org/10.1029/2009JA014069

Birn, J., & Hesse, M. (1996). Details of current disruption and diversion in simulations of magnetotail dynamics. *Journal of Geophysical Research*, *101*(A7), 15345–15358. https://doi.org/10.1029/96JA00887

Bonfond, B., Yao, Z. H., Gladstone, G. R., Grodent, D., Gérard, J.-C., Matar, J., et al. (2021). Are Dawn Storms Jupiter's Auroral Substorms? *AGU Advances*, *2*(1). http://dx.doi.org/10.1029/2020av000275

Clarke, J. T., Ballester, G., Trauger, J., Ajello, J., Pryor, W., Tobiska, K., et al. (1998). Hubble Space Telescope imaging of Jupiter's UV aurora during the Galileo orbiter mission. *Journal of Geophysical Research*, *103*(E9), 20217–20236.

Clarke, J. T., Gérard, J.-C., Grodent, D., Wannawichian, S., Gustin, J., Connerney, J., et al. (2005). Morphological differences between Saturn's ultraviolet aurorae and those of Earth and Jupiter. *Nature*, *433*(7027), 717–719.

Clarke, J. T., Grodent, D., Cowley, S. W. H., Bunce, E. J., Zarka, P., Connerney, J. E. P., & Satoh, T. (2004). Jupiter's Aurora. Jupiter: The Planet, Satellites and Magnetosphere (Vol. 1, 639–670).

Clarke, J. T., Nichols, J., Gérard, J.-C., Grodent, D., Hansen, K. C., Kurth, W., et al. (2009). Response of Jupiter's and Saturn's auroral activity to the solar wind. *Journal of Geophysical Research*, *114*(A5). https://doi.org/10.1029/2008JA013694

Connerney, J. E. P., Acuna, M. H., & Ness, N. F. (1981). Modeling the Jovian current sheet and inner magnetosphere. *Journal of Geophysical Research*, *86*(A10), 8370–8384.

Connerney, J. E. P., Benn, M., Bjarno, J., Denver, T., Espley, J., Jorgensen, J., et al. (2017). The Juno magnetic field investigation. *Space Science Reviews*, *213*(1–4), 39–138.

Connerney, J. E. P., Kotsiaros, S., Oliversen, R. J., Espley, J. R., Joergensen, J. L., Joergensen, P. S., et al. (2018). A new model of Jupiter's magnetic field from Juno's first nine orbits. *Geophysical Research Letters*, *45*(6), 2590–2596.

Cowley, S. W. H., Badman, S. V., Bunce, E., Clarke, J., Gérard, J.-C., Grodent, D., & Yeoman, T. K. (2005). Reconnection in a rotation-dominated magnetosphere and its relation to Saturn's auroral dynamics. *Journal of Geophysical Research*, *110*(A2). https://doi.org/10.1029/2004JA010796

Cowley, S. W. H., & Bunce, E. (2003). Modulation of Jupiter's main auroral oval emissions by solar wind induced expansions and compressions of the magnetosphere. *Planetary and Space Science*, *51*(1), 57–79.

Cowley, S. W. H., & Bunce, E. J. (2001). Origin of the main auroral oval in Jupiter's coupled magnetosphere–ionosphere system. *Planetary and Space Science*, *49*(10–11), 1067–1088.

Cowley, S. W. H., Bunce, E. J., Stallard, T. S., & Miller, S. (2003). Jupiter's polar ionospheric flows: Theoretical interpretation. *Geophysical Research Letters*, *30*(5).

Gérard, J.-C., Grodent, D., Dols, V., Prangé, R., Waite, J., Gladstone, G., & Jaffel, L. B. (1994). A remarkable auroral event on Jupiter observed in the ultraviolet with the Hubble Space Telescope. *Science*, *266*(5191), 1675–1678.

Gershman, D., DiBraccio, G., Connerney, J., Hospodarsky, G., Kurth, W., Ebert, R., et al. (2017). Juno observations of large-scale compressions of Jupiter's dawnside magnetopause. *Geophysical Research Letters*, *44*(15), 7559–7568.

Gray, R., Badman, S. V., Bonfond, B., Kimura, T., Misawa, H., Nichols, J., & Ray, L. (2016). Auroral evidence of radial transport at Jupiter during January 2014. *Journal of Geophysical Research: Space Physics*, *121*(10), 9972–9984.

Grodent, D., Clarke, J. T., Kim, J., Waite, J. H., Jr, & Cowley, S. W. H. (2003). Jupiter's main auroral oval observed with HST-STIS. *Journal of Geophysical Research*, *108*(A11). https://doi.org/10.1029/2003JA009921

Grodent, D., Gérard, J.-C., Clarke, J. T., Gladstone, G. R., & Waite, J. H. (2004). A possible auroral signature of a magnetotail reconnection process on Jupiter. *Journal of Geophysical Research*, *109*(A5). https://doi.org/10.1029/2003JA010341

Gustin, J., Bonfond, B., Grodent, D., & Gérard, J.-C. (2012). Conversion from HST ACS and STIS auroral counts into brightness, precipitated power, and radiated power for H2 giant planets. *Journal of Geophysical Research*, *117*(A7). https://doi.org/10.1029/2012JA017607

Gustin, J., Cowley, S. W. H., Gérard, J.-C., Gladstone, G. R., Grodent, D., & Clarke, J. T. (2006). Characteristics of Jovian morning bright FUV aurora from Hubble Space Telescope/Space Telescope Imaging Spectrograph imaging and spectral observations. *Journal of Geophysical Research*, *111*(A9). https://doi.org/10.1029/2006JA011730

Haynes, P., Balogh, A., Dougherty, M., Southwood, D., Fazakerley, A., & Smith, E. (1994). Null fields in the outer Jovian magnetosphere: Ulysses observations. *Geophysical Research Letters*, *21*(6), 405–408.

Hill, T. W. (2001). The Jovian auroral oval. *Journal of Geophysical Research*, *106*(A5), 8101–8107.

Hospodarsky, G., Kurth, W., Bolton, S., Allegrini, F., Clark, G., Connerney, J., et al. (2017). Jovian bow shock and magnetopause encounters by the Juno spacecraft. *Geophysical Research Letters*, *44*(10), 4506–4512.

Kane, M., Mauk, B., Keath, E., & Krimigis, S. (1995). Hot ions in Jupiter's magnetodisc: A model for Voyager 2 low-energy charged particle measurements. *Journal of Geophysical Research*, *100*(A10), 19473–19486.

Khurana, K. K. (1992). A generalized hinged-magnetodisc model of Jupiter's nightside current sheet. *Journal of Geophysical Research*, *97*(A5), 6269–6276.

Khurana, K. K., & Schwarzl, H. K. (2005). Global structure of Jupiter's magnetospheric current sheet. *Journal of Geophysical Research*, *110*(A7). https://doi.org/10.1029/2004JA010757

Kim, T. K., Ebert, R., Valek, P., Allegrini, F., McComas, D., Bagenal, F., et al. (2020). Method to derive ion properties from Juno JADE including abundance estimates for O+ and S2+. *Journal of Geophysical Research: Space Physics*, *125*(2), e2018JA026169. https://doi.org/10.1029/2018JA026169

Kimura, T., Nichols, J. D., Gray, R., Tao, C., Murakami, G., Yamazaki, A., et al. (2017). Transient brightening of Jupiter's aurora observed by the Hisaki satellite and Hubble Space Telescope during approach phase of the Juno spacecraft. *Geophysical Research Letters*, *44*(10), 4523–4531.

Kivelson, M., & Southwood, D. (2005). Dynamical consequences of two modes of centrifugal instability in Jupiter's outer magnetosphere. *Journal of Geophysical Research*, *110*(A12). https://doi.org/10.1029/2005JA011176

Kurth, W., Hospodarsky, G., Kirchner, D., Mokrzycki, B., Averkamp, T., Robison, W., & Zarka, P. (2017). The Juno waves investigation. *Space Science Reviews*, *213*(1–4), 347–392.

Leamon, R., Dougherty, M., Southwood, D., & Haynes, P. (1995). Magnetic nulls in the outer magnetosphere of Jupiter: Detections by Pioneer and Voyager spacecraft. *Journal of Geophysical Research*, *100*(A2), 1829–1835.

Lui, A. (1996). Current disruption in the Earth's magnetosphere: Observations and models. *Journal of Geophysical Research*, *101*(A6), 13067–13088.

Lui, A. (2009). Comment on tail reconnection triggering substorm onset. *Science*, *324*(5933), 1391.

Mauk, B., Cohen, I., Haggerty, D., Hospodarsky, G., Connerney, J., Anderson, B., et al. (2019). Investigation of mass-/charge-dependent escape of energetic ions across the magnetopauses of Earth and Jupiter. *Journal of Geophysical Research: Space Physics*, *124*. https://doi.org/10.1029/2019JA026626

Mauk, B., Haggerty, D., Jaskulek, S., Schlemm, C., Brown, L., Cooper, S., et al. (2017). The Jupiter energetic particle detector instrument (JEDI) investigation for the Juno mission. *Space Science Reviews*, *213*(1–4), 289–346.

McComas, D., Alexander, N., Allegrini, F., Bagenal, F., Beebe, C., Clark, G., et al. (2017). The Jovian auroral distributions experiment (JADE) on the Juno Mission to Jupiter. *Space Science Reviews*, *213*(1–4), 547–643.

Nichols, J. D., Badman, S. V., Bagenal, F., Bolton, S. J., Bonfond, B., Bunce, E. J., et al. (2017). Response of Jupiter's auroras to conditions in the interplanetary medium as measured by the Hubble Space Telescope and Juno. *Geophysical Research Letters*, *44*(15), 7643–7652.

Nichols, J. D., Badman, S. V., Baines, K., Brown, R., Bunce, E., Clarke, J., et al. (2014). Dynamic auroral storms on Saturn as observed by the Hubble Space Telescope. *Geophysical Research Letters*, *41*(10), 3323–3330.

Nichols, J. D., Clarke, J. T., Gérard, J.-C., Grodent, D., & Hansen, K. C. (2009). Variation of different components of Jupiter's auroral emission. *Journal of Geophysical Research*, *114*(A6). https://doi.org/10.1029/2009JA014051

Radioti, A., Grodent, D., Gérard, J.-C., & Bonfond, B. (2010). Auroral signatures of flow bursts released during magnetotail reconnection at Jupiter. *Journal of Geophysical Research*, *115*(A7). https://doi.org/10.1029/2009JA014844

Radioti, A., Grodent, D., Gérard, J.-C., Bonfond, B., & Clarke, J. (2008). Auroral polar dawn spots: Signatures of internally driven reconnection processes at Jupiter's magnetotail. *Geophysical Research Letters*, *35*(3).

Radioti, A., Grodent, D., Gérard, J.-C., Vogt, M., Lystrup, M., & Bonfond, B. (2011). Nightside reconnection at Jupiter: Auroral and magnetic field observations from 26 July 1998. *Journal of Geophysical Research*, *116*(A3). https://doi.org/10.1029/2010JA016200

Southwood, D. J., Dougherty, M., Canu, P., Balogh, A., & Kellogg, P. J. (1993). Correlations between magnetic field and electron density observations during the inbound Ulysses Jupiter flyby. *Planetary and Space Science*, *41*(11–12), 919–930.

Southwood, D. J., & Kivelson, M. G. (2001). A new perspective concerning the influence of the solar wind on the Jovian magnetosphere. *Journal of Geophysical Research*, *106*(A4), 6123–6130.

Vogt, M. F., Bunce, E. J., Kivelson, M. G., Khurana, K. K., Walker, R. J., Radioti, A., & Grodent, D. (2015). Magnetosphere-ionosphere mapping at Jupiter: Quantifying the effects of using different internal field models. *Journal of Geophysical Research: Space Physics*, *120*(4), 2584–2599. https://doi.org/10.1002/2014JA020729

Vogt, M. F., Kivelson, M. G., Khurana, K. K., Walker, R. J., Bonfond, B., Grodent, D., & Radioti, A. (2011). Improved mapping of Jupiter's auroral features to magnetospheric sources. *Journal of Geophysical Research*, *116*(A3). https://doi.org/10.1029/2010JA016148

Woch, J., Krupp, N., & Lagg, A. (2002). Particle bursts in the Jovian magnetosphere: Evidence for a near-Jupiter neutral line. *Geophysical Research Letters*, *29*(7), 42-1–42-4. https://doi.org/10.1029/2001GL014080

Yao, Z., Bonfond, B., Clark, G., Grodent, D., Dunn, W., Vogt, M., & others (2020). Reconnection and dipolarization driven auroral dawn storms and injections. *Journal of Geophysical Research: Space Physics*, *125*, e2019JA027663. https://doi.org/10.1029/2019JA027663